ELSEVIER

International Journal of Applied Earth Observation and Geoinformation 7 (2005) 163–182

INTERNATIONAL JOURNAL OF APPLIED EARTH OBSERVATION AND GEOINFORMATION

www.elsevier.com/locate/jag

Extraction of morphotectonic features from DEMs: Development and applications for study areas in Hungary and NW Greece

G. Jordan [a,b,c,*], B.M.L. Meijninger [d], D.J.J. van Hinsbergen [d], J.E. Meulenkamp [d], P.M. van Dijk [e]

[a] *Joint Research Centre of the European Commission, Ispra, Italy*
[b] *Geological Institute of Hungary, Stefania ut 14, Budapest 1143, Hungary*
[c] *Uppsala University, Institute for Earth Sciences, Uppsala, Sweden*
[d] *Vening Meinez Research School of Geodynamics, Faculty of Geosciences, Utrecht University, The Netherlands*
[e] *ITC International Institute for Geo-Information Science and Earth Observation, Enschede, The Netherlands*

Received 23 December 2003; accepted 7 March 2005

Abstract

A procedure for the consistent application of digital terrain analysis methods to identify tectonic phenomena from geomorphology is developed and presented through two case studies. Based on the study of landforms related to faults, geomorphological characteristics are translated into mathematical and numerical algorithms. Topographic features represented by digital elevation models of the test areas were extracted, described and interpreted in terms of structural geology and geomorphology. Digital terrain modelling was carried out by means of the combined use of: (1) numerical differential geometry methods, (2) digital drainage network analysis, (3) digital geomorphometry, (4) digital image processing, (5) lineament extraction and analysis, (6) spatial and statistical analysis and (7) digital elevation model-specific digital methods, such as shaded relief models, digital cross-sections and 3D surface modelling. A sequential modelling scheme was developed and implemented to analyse two selected study sites, in Hungary and NW Greece on local and regional scales. Structural information from other sources, such as geological and geophysical maps, remotely sensed images and field observations were analysed with geographic information system techniques. Digital terrain analysis methods applied in the proposed way in this study could extract morphotectonic features from DEMs along known faults and they contributed to the tectonic interpretation of the study areas.

Keywords: Digital elevation model; Digital terrain modelling; Morphometry; Structural geology; Tectonic geomorphology

* Corresponding author. Tel.: +36 1 251 0999/223; fax: +36 1 251 0703.
E-mail address: jordan@mafi.hu (G. Jordan).

0303-2434/$ – see front matter © 2005 Elsevier B.V. All rights reserved.
doi:10.1016/j.jag.2005.03.003

1. Introduction

Surface methods such as remote sensing and morphological analysis provide fast and relatively cheap information, complementary to classical field geology in order to study subsurface geology. Morphological analysis of topographic features, in particular lineaments, has long been applied in structural and tectonic studies (Hobbs, 1912; Frisch, 1997) and has become a fundamental tool in tectonic analyses using (stereo-) aerial photographs and other remotely sensed imagery (Siegal and Gillespie, 1980; Drury, 1987; Salvi, 1995). Although the interpretation of land morphology in terms of geological structures is well-established (Prost, 1994; Keller and Pinter, 1996) there is yet no case study documented in the literature involving the consistent application of available digital terrain analysis methods for tectonic geomorphology.

Most of the tectonic studies applying digital terrain models use shaded relief models either alone (Simpson and Anders, 1992; Byrd et al., 1994; Collet et al., 2000) or in combination with remotely sensed images on a regional scale (Florinsky, 1998; Chorowicz et al., 1999). Three-dimensional view with image drape (Le Turdu et al., 1995) and digital cross-sections (Chorowicz et al., 1998) have been used for morphotectonic investigations. Chorowicz et al. (1991) used a digital elevation model (DEM) to calculate dip and strike from geological maps and Koike et al. (1998) calculated fault plane geometries from DEMs. Onorati et al. (1992) used slope and aspect calculations in a regional morphotectonic investigation. Florinsky (1996) studied the relationship between fault type and landforms and used curvature maps to recognise and characterise fault lines. Chorowicz et al. (1989, 1995) studied strike-ridge geomorphology and used profile geometry for its recognition in the DEM. Riley and Moore (1993) used elevation histogram to identify horizontal pediments on mountain slopes associated with normal faulting. Trend analysis has been used to study tectonically induced tilt (Doornkamp, 1972; Fraser et al., 1995; Guth, 1997), and spectral analysis has been used for the investigation of landform periodicities (Harrison and Lo, 1996). The most important limitations of many of these studies are that: (1) most of the studies use a single method (or only a few methods) for feature recognition and description, (2) all of the studies are at the regional scale, although landform observations are at the local scale, (3) most of the studies use visual methods of feature (mostly lineament) extraction, (4) there are very few cases involving the analysis and extraction of landforms specific to tectonic structures, (5) most of the methods can be applied to neo-tectonic landforms only and (6) there is a lack of rigorous study of the relationship between tectonic processes, secondary geological processes and their representation in DEMs.

Systematic digital tectonic geomorphology analysis is hampered by: (1) the lack of such studies in literature and (2) the non-uniform description and use of relevant digital methods in different fields of the Earth Sciences. Essentially identical methods are often used in these different fields with different names and for different purposes that makes their adoption to digital tectonic geomorphology difficult. For example, calculated gradients are used as edge enhancement filters in digital image processing while they have direct geometric implications in geomorphometry. Numerical operators have different names in the different fields of study. For example, Prewitt operators (Prewitt, 1970) of image analysis are called ‘Sharpnack and Akin (1969) gradient filter’ or ‘six-term quadratic model’ in the terrain modelling literature, all being equal to a least-squares linear trend fit to the nine grid neighbours. Similarly, valley network extraction is a tool in differential geometry studies as well as in hydrological modelling. Analysis of directional data is crucial in image processing, hydrology, mathematical and structural geology. Histogram analysis is a basic tool in both image processing and geomorphometry. Image analysis methods are often applied to grey-scale terrain models, thus losing inherent geometric information. Accordingly, available software designed for the specific needs of each field of study does in many cases not offer all the operations required for consistent digital terrain analysis. Geographic information system (GIS) software can easily perform most of the analyses but some procedures may be very difficult to implement. Digital analysis of the kind presented here requires the use of an integrated system of many analytical and software tools.

Digital tectonic geomorphology is the integration of three components: structural geology, geomorphology and digital terrain analysis (DTA) (Jordan and

Csillag, 2001, 2003). There is, however, a gap between structural geology and DTA. The objective of this study is to provide an overview of methods for the extraction of morphotectonic features from DEMs and to develop a systematic procedure for the application of these methods to morphotectonic terrain analysis. In this paper, discussion is limited to the analysis of faults. In view of the great diversity of morphotectonic features (Keller and Pinter, 1996; Burbank and Anderson, 2001), only a limited selection of fault-related landforms is discussed. The emphasis of this study, however, is on digital data processing. Detailed tectonic geomorphology interpretations of the presented examples are provided elsewhere (Jordan et al., 2003).

2. Methods

2.1. Geometric and spatial analysis of morphological features associated with fractures

Structural discontinuities in rocks most often result in linear morphological features along the intersection of fracture plane and land surface. Linear morphological expressions of fractures include: (1) linear valleys, (2) linear ridgelines and (3) linear slope-breaks. The main geometric characteristics of a *single* linear line are orientation and length (continuity) and in case of curved line, curvature (Fig. 1A) (Jordan and Csillag, 2003). Linear fracture traces are most obvious in the case of high-dip faults of normal, reverse and strike-slip type while thrust faults tend to appear irregular in topography (Prost, 1994; Drury, 1987; Goldsworthy and Jackson, 2000). Intersection of topographic surface and fold structures can also result in linear and planar features depending on the geometry and orientation of the folds with respect to the erosion surface (Ramsay and Huber, 1987).

Planar features such as uniform hillsides also develop along fractures. Geometry of planar surfaces are described by uniform aspect and high and constant slope values (Fig. 1A). Shape and area extent are also important characteristics. Large elongated areas of uniform aspect and slope with linear boundaries can be associated with faults. The measure of curvature is important in cases of complex curving fracture surfaces.

Specific geomorphological features forming along faults are diverse (Burbank and Anderson, 2001). For example, asymmetric geometry of slopes across valley and ridgeline axes, as measured by uniform slope angle differences, can result from tectonic influences on the morphology. Characteristic landforms, such as depressions, pressure bulges or tilt of flats is commonly seen in fault zones. Depressions and bulges are geometric locations of local elevation minima and maxima, respectively. Characteristic shape and slope conditions describe their geometry (Keller and Pinter, 1996). Tilt of flats result in uniform surface gradients.

Most of the above morphological features, such as linear valley lines, asymmetric slopes and depressions may be caused by secondary processes or can be associated with lithology. For example, wind erosion may create linear patterns; planar surfaces, linear valleys and ridges and asymmetric slopes are often associated with bedding and linear morphological features may arise from lithological contacts between different rock types (Way, 1973).

The spatial relationships *among* fractures can be described either statistically by a spatial frequency analysis of the above characteristics or topologically (Fig. 1A). In statistical analysis, location of individual features is not considered within the studied population. For example, angular statistics (rose diagrams) are used for analysis of orientation distribution in the study area. Another approach in many-fracture analysis considers fracture populations as networks and focuses on their pattern of intersection in terms of lengths, angle and frequencies, mutual dislocations and shape and size of fracture-bounded areas, from which the stress field can be quantified (Ramsay and Huber, 1987). This approach is commonly known as topological analysis, where the location and relationships of individual features are considered (Fig. 1A).

Lithological structures within rock units may also be represented by DEMs and their description might help clarifying geological and structural relationships, but these features can also obscure tectonic structures. Intersection of bedding and the topography can appear as linear line features or planar features in digital terrain models (DTMs). Curved or even circular patterns are most commonly associated with plutons, volcanic cones and calderas, as shown in the case studies below. The contacts and spatial relationship among rock units

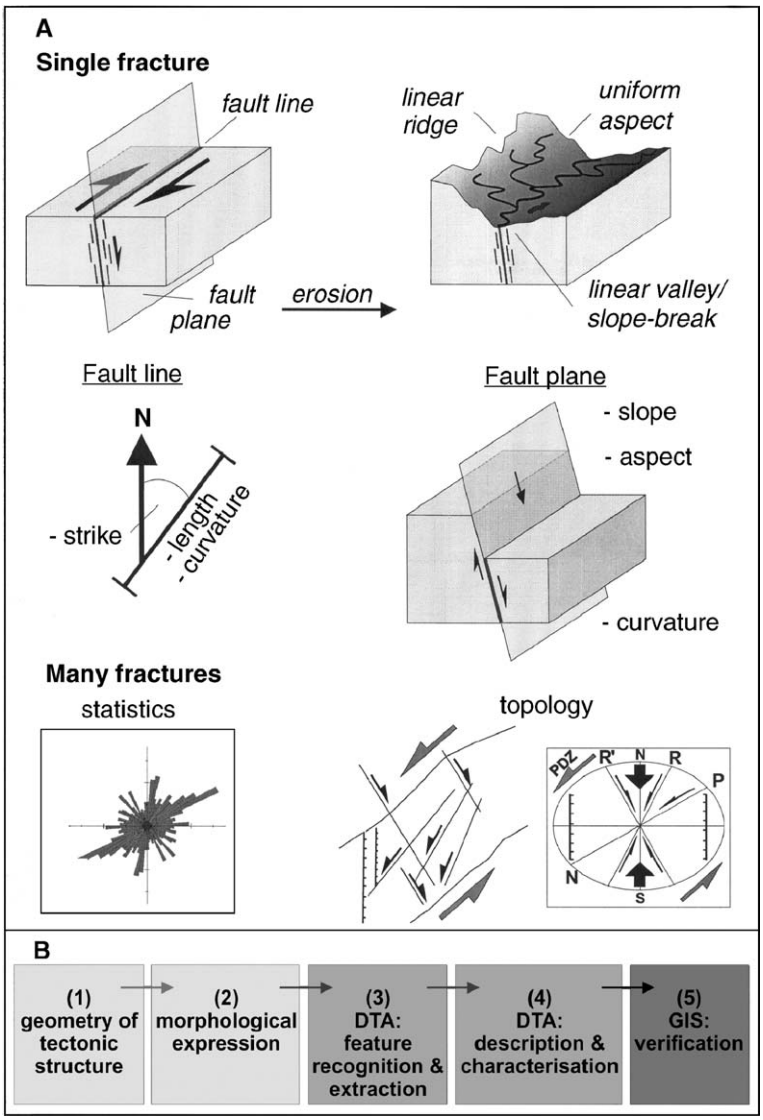

Fig. 1. (A) Geometric and spatial analysis of fractures. (B) Analytical steps in digital tectonic geomorphology. See text for details.

may equally result in linear or curved features that can only be distinguished from lines of tectonic origin via geological information from other sources.

Secondary geomorphological indicators of tectonic influence are dislocations of geomorphic surfaces, such as erosional surfaces and alluvial plains, and these surfaces are the result of uplift, subsidence or tilting. Fluvial networks are the most common indicators; the drainage network pattern reflects often the regional or even the local tectonic framework. Parallel-running streams could indicate a tilted block and thus the presence of a listric normal fault, oriented perpendicular to the flow direction of these streams. Likewise, large strike-slip fault zones commonly show linear arrangements of depressions and lakes.

In the absence of further morphological evidence, these secondary morphological features can be distinguished from features of non-tectonic origin with the use of geological information. Geological data from various sources, such as geological maps, geophysical

data, remotely sensed images and field measurements also have to be incorporated in the GIS database.

2.2. Feature recognition and parameter extraction from DEMs for tectonic geomorphology

In order to maximise the tectonic geomorphology information obtained from a DEM, a sequential modelling scheme (Jordan and Csillag, 2001, 2003) was applied in this study. The design of the modelling scheme was based on the following considerations:

- the objective is the quantitative geometric characterisation of landforms;
- the objective is providing reproducible outputs;
- analysis proceeds from simple to the more complex methods;
- outputs from modelling steps are controlled by input data and parameters;
- the procedure integrates a wide-range of available methods;
- multi-source information is integrated in the database;
- DTA is implemented in a GIS environment.

The components of digital tectonic geomorphology in this study were: (1) numerical differential geometry, (2) digital drainage network analysis, (3) digital geomorphometry, (4) digital image processing, (5) lineament extraction and analysis, (6) spatial and statistical analysis and (7) DEM-specific digital methods, such as shaded relief models, digital cross-sections and 3D surface modelling. Fig. 1B illustrates the procedure of recognition and extraction of fault-related landforms and their tectonic interpretation. Based on the study of landforms related to faults (see Section 2.1), geomorphological characteristics were translated into mathematical and numerical algorithms. Topographic features represented by DEMs of test areas were extracted and characterised by DTA (Fig. 1B). Verification of structural implications used complementary data sources in GIS.

The analysis in this study proceeded from simple univariate elevation studies, through differential geometric surface analysis and drainage network analysis, to the multivariate interpretation of results using GIS technology (Fig. 2). Reproducibility of morphological analysis was achieved by the application of numerical data processing algorithms. Each modelling module (Fig. 2) had a set of defined input parameters. Subsequent steps were based on output of previous terrain models. Prior to the spatial analysis of each terrain attribute, its histogram was studied for systematic error and statistical properties, such as multi-modality. Histograms were interpreted in terms of morphometry and used for classification of terrain data. Image stretching for enhancement of visual interpretation was also based on histograms.

2.2.1. Analysis of elevation data

Terrain data calculated from DEMs are influenced by data source, interpolation method and gradient calculation algorithm (Moore et al., 1993). Among interpolation methods, Triangular Irregular Network (TIN) interpolation can represent sudden changes in topography which is particularly useful in tectonic geomorphology (McCullagh, 1988). Moreover, TINs are efficient in the representation of areas with uniform aspect, essential for identification of tectonically induced erosion morphology of spurs and pediments (Riley and Moore, 1993).

Digitised contour lines were used as elevation data source for the study areas causing systematic errors in elevation, slope and profile curvature data but having little effect on aspect calculations. In order to account for the effects of various interpolation methods, DEMs calculated from contour lines using TIN interpolation were compared to the original DEM grids for the study areas.

The simplest morphological analysis involves the study of elevation data (Fig. 2A). In the present approach, DEMs were displayed for visual inspection as contour maps, grey-scale images, 3D surface views, shaded relief models or as combinations of these. The shaded relief model was a key component throughout this study because it was the most suitable terrain model for the recognition and interpretation of complex morphological features. Vertical exaggeration of elevations was used to enhance the study of subtle features in flat basin areas, and cross-sections were generated along geological sections to study slope and slope curvature conditions. The parameters studied in elevation cross-sections were slope (first derivative), change in slope (second derivative) and slope convexity (sign of second derivative) (Fig. 2A).

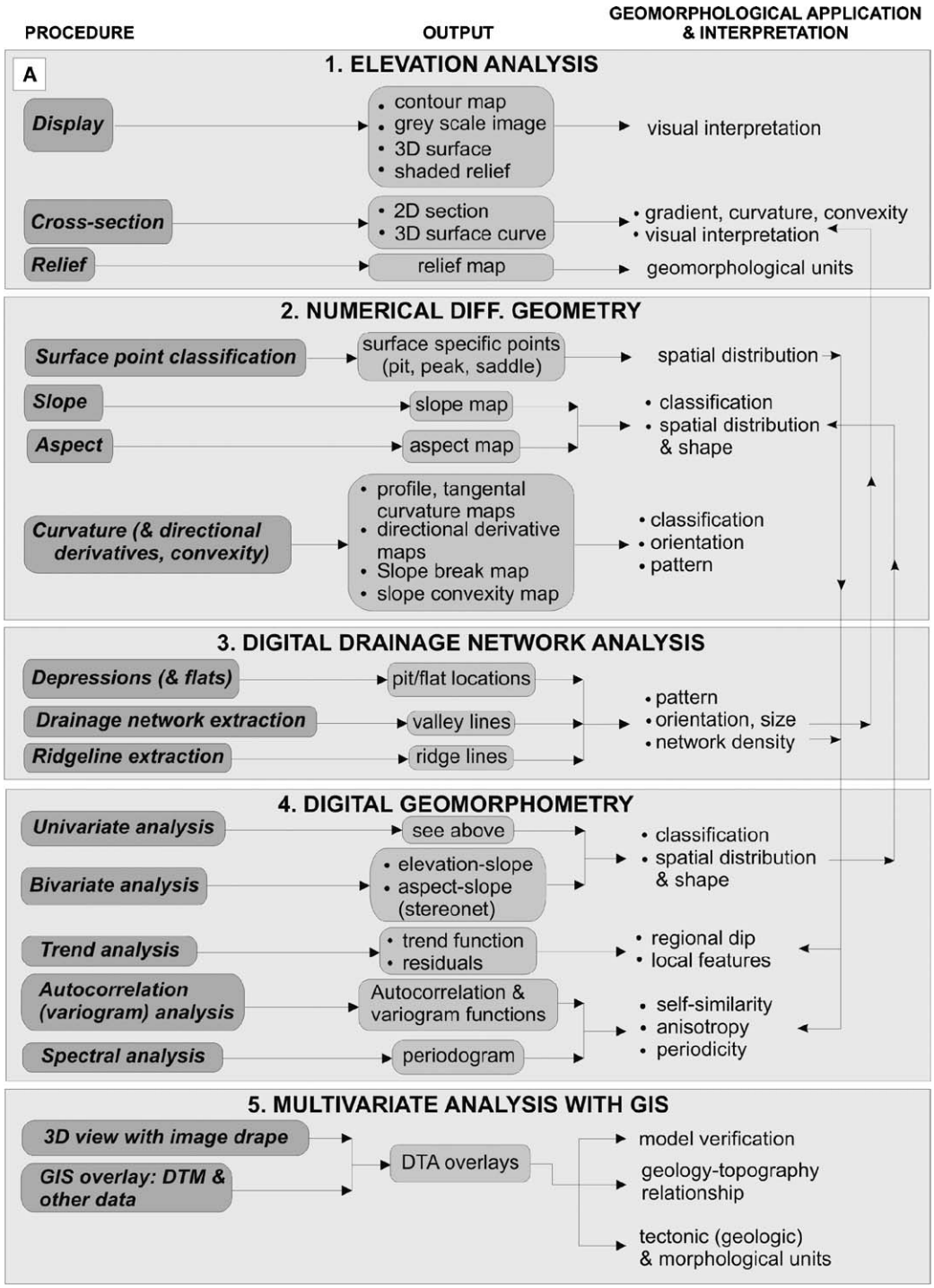

Fig. 2. A digital terrain analysis procedure for systematic study of tectonic geomorphology features in DEMs. (A) Flow chart of numerical methods. (B) Image processing methods applied to terrain models.

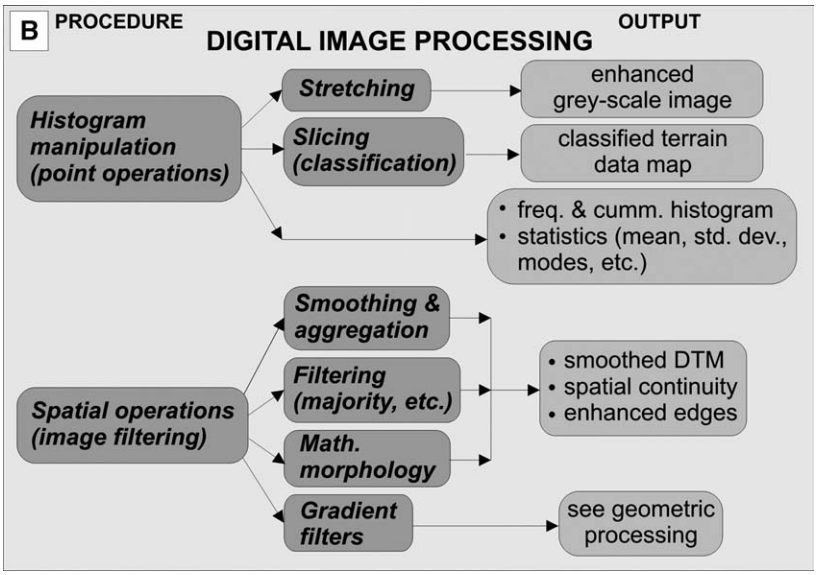

Fig. 2. (*Continued*).

2.2.2. Numerical differential geometry calculations

The localization of surface-specific points, i.e. local maxima (peaks), minima (pits), saddle points (passes) and slope-breaks, is fundamental in digital geomorphologic analysis (Peucker and Douglas, 1975). Peaks and pits were calculated using simple 'higher than' algorithms (Garbrecht and Martz, 1995). In this study, local maxima (peaks) were used for the analysis of regional tilt by means of trend fitting, passes were defined as local minima along ridges (watershed divides) identified by digital drainage network analysis (see below), and slope-breaks were defined as slope changes above a predefined threshold of profile curvature. Valley and ridge lines were extracted by means of digital drainage analysis methods (Jordan and Csillag, 2001).

In this study, terrain aspect, second-order directional derivatives and curvatures were calculated for regular points only, while inflex points were not considered for morphotectonic interpretation. The digital model of topography generated by interpolation can be regarded as a $z = f(x,y)$ bivariate function and hence analysed by means of differential geometry (Moore et al., 1993). Introducing the following notations (after Mitášová and Hofierka, 1993) and assuming that the continuous second-order partial derivatives of the function f exist:

$$fx = \frac{\partial z}{\partial x}, \qquad fy = \frac{\partial z}{\partial y}, \qquad fxx = \frac{\partial^2 z}{\partial x^2},$$

$$fyy = \frac{\partial^2 z}{\partial y^2}, \qquad fxy = \frac{\partial^2 z}{\partial x \partial y}$$

and

$$p = f^2x + f^2y, \qquad q = p + 1$$

the magnitude of the gradient vector ($\bigtriangledown f = \mathbf{grad}(fx, fy)$) is $|\mathbf{grad}| = (f^2x + f^2y)^{1/2}$ from which the steepest slope angle is computed as:

$$\gamma = \arctan\sqrt{p},$$

and aspect is given by

$$\alpha = 180^\circ - \arctan\left(\frac{fy}{fx}\right) + 90\left(\frac{fx}{|fx|}\right),$$

where azimuth is in degrees and measured clockwise from north.

Profile curvature (curvature of normal plane section in gradient direction) is defined as

$$k_p = \frac{fxx\, f^2x + 2\, fxy\, fx\, fy + fyy\, f^2y}{p\sqrt{q^3}},$$

and tangential curvature (measured in the normal plane in a direction perpendicular to the gradient) is given by:

$$k_t = \frac{fxx\, f^2y - 2\, fxy\, fx\, fy + fyy\, f^2x}{p\sqrt{q}}.$$

Profile curvature reflects the change in slope angle and was used to define slope-breaks for tectonic geomorphology interpretation. Tangential curvature is measured in a direction perpendicular to the gradient and hence reflects the change in aspect angle. Ridge and valley lines are often represented by high values of tangential curvature. The convexity of slopes is expressed by the sign and magnitude of curvatures (Mitášová and Hofierka, 1993; Florinsky, 2000). Second-order derivatives in the axial directions (*fxx* and *fyy*) and mixed second-order derivative (*fxy*) were used to identify slope-breaks in the four principle directions. First-order derivatives used the Prewitt operators for their smoothing effect (Gonzalez and Woods, 1993) while second-order derivatives used the scheme of ILWIS GIS (1997).

2.2.3. Digital drainage network analysis

Drainage network analysis is a fundamental tool in tectonic geomorphology (Deffontaines and Chorowicz, 1991). Fractures represent zones of rock weaknesses prone to intense erosion and hence valleys form along fault lines. Consequently, flow path routing and drainage network algorithms used in hydrological modelling can be applied for the purpose of morphological fracture tracing and network analysis (Fig. 2A).

Drainage network extraction in this study was carried out with the TOPAZ model developed by Martz and Garbrecht (1992). The network identified with this method provided fully connected, convergent and unidirectional down-slope channel network. Mathematical morphological methods of network skeletonisation were applied in two steps to eliminate erroneous parallel channels and to arrive at a single-pixel wide channel network. Skeletonisation was preceded by filling gaps between erroneous diagonal parallel channels and by anchoring of original channel source pixels using mathematical morphology procedures (Gonzalez and Woods, 1993). The skeletonised network was then burnt into the depression-filled DEM by extracting 20 m from channel pixel elevations to account for the 10 m contour line separation in the Kali Basin study area. Elevations along the burnt channel segments were smoothed with a 3×3 moving average filter. Automated channel extraction performed on the thus processed DEM resulted in a high-density, single-pixel wide drainage network with ridgelines correctly positioned on hill crests (Jordan, 2003) (Fig. 2A). The obtained drainage and ridge network was used in all subsequent analyses.

The binary image of the channel network extracted in the above way was used in this study to create an artificial elevation model of valleys (Jordan, 2003). Single-pixel wide channel lines were widened with morphological dilatation using a 3×3 structuring element (Gonzalez and Woods, 1993). Background pixels were assigned zero, channel pixels received a constant elevation value and the resulting three-pixel wide drainage valleys were smoothed with a 3×3 average filter. The resulting valley network shown in this study had uniform depth and was used for analysis of periodicity.

2.2.4. Digital geomorphometry analysis

Elevation and derivatives of altitude formed the bases for the geomorphometric study in this investigation (Evans, 1972). According to Evans (1980), the five basic parameters calculated are elevation, slope, aspect, profile and tangential curvatures. Univariate analysis involves the study of statistical and spatial distribution of the basic parameters. In this study, a peak in the aspect frequency histogram or a large petal in a rose diagram showed that a larger number of pixels had aspect in a preferred orientation. Where these pixels formed one or more connected areas on hillsides with linear boundaries, a tectonic origin could be inferred.

Next in the analysis, bivariate and multivariate relationships between variables (derivatives and moments) were studied (Fig. 2A). Slopes and aspects were plotted in a stereonet to study if steep slopes had preferred orientations, as steep slopes with the same orientation may be associated with faulting. Relief map was calculated in this study as the quotient of the local standard deviation and average elevations in a moving kernel applied to the regional-scale DEMs.

Finally, terrain ‘texture’ was studied by means of spatial statistical methods and network analysis

techniques. Trend analysis, autocorrelation and spectral analysis were carried out for the entire area or specific parts of the area (e.g. basins only, Fig. 2A). The trend surface was fitted to all data points or to surface-specific points, such as peaks or valley lines, to estimate regional dips, as the tilt of an area is often related to tectonic movements. Spectral analysis resulted in a two-dimensional periodogram that identified dominant periodicities as significant local maxima in the diagram (Davis, 1986; Jordan and Schott, 2005).

Autocorrelation and spectral analyses revealed lineation (anisotropy) and periodicity of a landscape due to faulting or folding (Jordan and Schott, 2005). The autocorrelation property was also studied by calculating semi-variograms in different directions (Curran, 1988). Problems emerged from the fact that valleys often curve and there are confluences down-valley, and that ridge height and spacing may vary (Evans, 1972). In order to overcome the problem of converging ridges of alternating height, analysis in this study was limited to valley lines only, as defined by the digital drainage network identification method described above.

2.2.5. Digital image processing of terrain data

DEMs and each derived attribute map can be viewed as raster images and hence be processed using digital image processing procedures to increase the apparent distinction between features in the scene (Sauter et al., 1989, Fig. 2B). Point operations of histogram slicing and contrast stretching had two applications in this study. Slicing of an image histogram by dividing pixel values into specified intervals was used here to display discrete categories of elevation, slope, aspect and other terrain attributes (Lillesand and Kiefer, 1994; see Fig. 2B). Aspect data were displayed and analysed by means of rose diagrams and circular statistics (Wells, 1999; Baas, 2000). Areas of uniform terrain attribute were then examined for spatial distribution, continuity and shape while contrast stretching was performed on grey-level images to enhance visual interpretations of the terrain models (Lillesand and Kiefer, 1994) (Fig. 2B).

In this study, local operators of gradient filters as discussed above (Fig. 2A and B) were applied only to terrain data and not to grey-scale images in order to preserve the original geometric information in terrain models. In this way, valleys, ridges and slope-breaks were extracted on geometric bases. For example, slope-breaks were recognised as edges if the change in slope in the gradient direction (profile curvature) exceeded a predefined threshold. In this study, moving average filters were used to reduce noise in elevation models. Filter kernel size for smoothing was selected on the basis of the scale of the feature to be studied. When the studied features had various scales (e.g. hill slopes), appropriate kernel size was selected on visual basis by comparing results of successive smoothing of DEM. Extraction of areas of same terrain attribute (e.g. aspect angle) were enhanced by applying majority filters to the terrain attribute map that assign the predominant value to the central pixel in the kernel. Image processing techniques, such as smoothing (low-pass filtering), image filtering or histogram slicing were carried out at almost all stages of the analysis (Fig. 2B).

Hill shading methods producing relief maps are peculiar to DEM images and are fundamental for morphostructural analysis (Simpson and Anders, 1992). Hill shading increases the contrast of very subtle intensity variations of an image, much more than contouring or pseudo-colour representation do (Drury, 1987). Onorati et al. (1992) used multi-image operation of false colour composites (i.e. red, green and blue colour components) in morphotectonic studies to simultaneously analyse three DTMs. In the present study, colour-separated geological maps and remotely sensed images were combined with a shaded relief map. These in turn were draped on the three-dimensional perspective view of the study areas to enable the study of the relationship between geology and morphology.

2.2.6. Spatial analysis of lineaments

Lineaments are defined as straight linear elements, visible at the earth's surface, which are the representations of geological and/or geomorphological phenomena (Clark and Wilson, 1994). In geomorphometric analysis, a linear feature may have geometric origin only and represent a change in terrain elevation, such as a valley or ridgeline, slope-break or inflex line. In terms of digital modelling, a lineament is a continuous series of pixels having similar terrain values (Koike et al., 1998). Each line was characterised by length and orientation in this study (Fig. 1A). Spatial distribution

and relationships among lines were described by length and orientation frequencies calculated for the entire area or sub-areas (Fig. 1A). In the present case studies, lineament intersection density, total length per area and frequency per area were analysed. Two lineament extraction procedures were applied in this study: (1) an automatic procedure using digital drainage extraction to identify valley and ridgelines and (2) interactive lineament interpretation of terrain models. In the case studies below, the nature of a lineament was assessed on the basis of field observations.

3. Study areas

3.1. Kali Basin, Hungary

The Kali Basin is located in the south-western part of the Balaton Highland in the Carpatho-Pannonian region (Trunko, 1995; Budai et al., 1999) (Fig. 3). The southern bordering hills are made up by folded Permian red sandstone. In the central and eastern parts, gently folded Triassic sediments are exposed. The majority of the basin is filled with horizontally bedded Tertiary clastic sediments. Late Miocene to Pliocene basaltic volcanics occur in the northern and western parts of the area (Fig. 3A). SE-verging reverse faults in the northern domain and folds in the southern part formed during the Cretaceous (Fig. 3A). Strike-slip faulting dominated in the region during the Miocene, and extensional tectonics characterised the latest Tertiary (Late Miocene and Pliocene). At present, the area is seismically inactive.

The specific objective in this study of the Kali Basin is the extraction and characterisation of morphological features associated with known faults on a local scale. A DEM of the Kali Basin was obtained from the national DTA-50 digital grid elevation database, initially produced via a third-

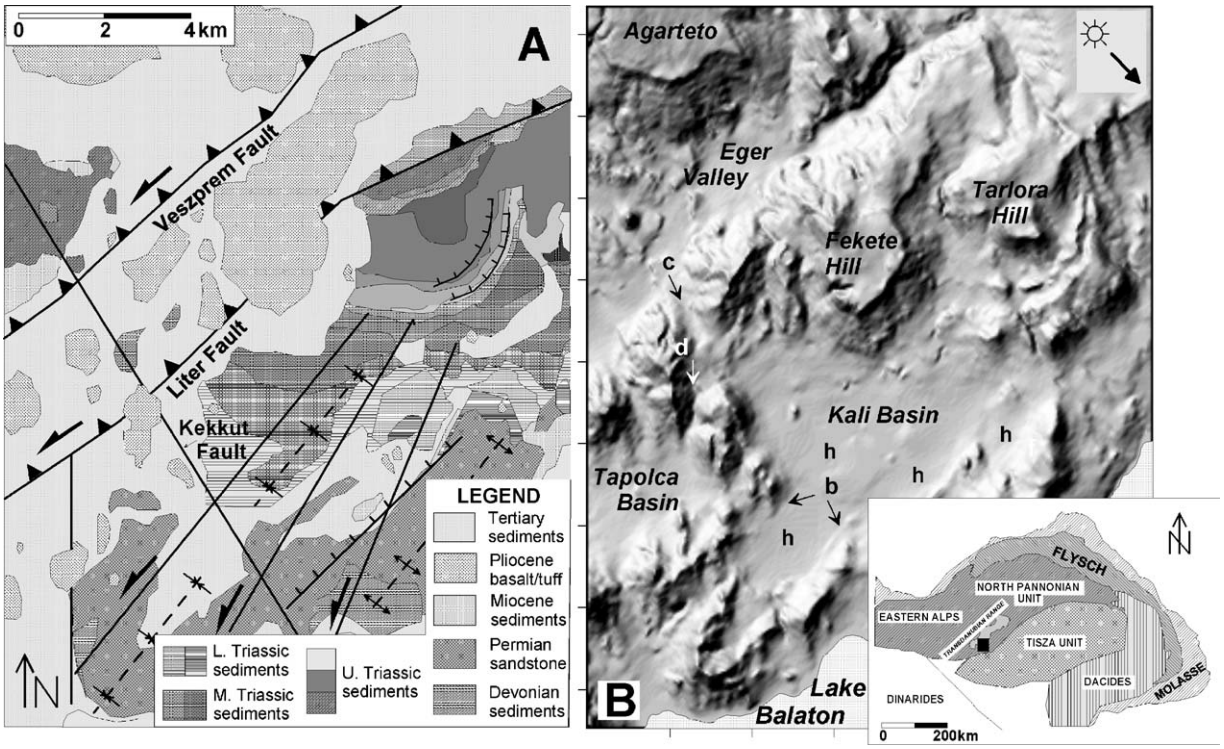

Fig. 3. Kali basin study area. (A) Geological map. Fault lines and fold axes indicated in geological maps are shown. (B) Shaded relief model (6× vertical exaggeration). Solid arrow indicates illumination direction. Letters highlight specific features. Inset: location of the study area in the Pannonian Basin, Hungary (solid rectangle). See text for details.

order spline function to interpolate from an original dataset of 10 m contour lines. The horizontal resolution of the grid is 50 m × 50 m and the vertical resolution is 1 m. Elevations above sea level are given as integers in meters.

3.2. NW Greece

A second case study was carried out in NW Greece, which exposes a NW–SE striking nappe pile (Fig. 4A) associated with African–Eurasian convergence in the course of the Late Mesozoic and Tertiary. The nappes themselves are internally highly folded and thrusted. The age of nappe emplacement becomes progressively younger from east to west, subdivided in the (pre-) Apulian zone (autochton) at the base of the tectonostratigraphy, overlaid by the Ionian zone, the Tripolitza zone and the Pindos zone (Aubouin, 1957; Bonneau, 1984) (Fig. 4A). Each of these zones consists of a Mesozoic to Lower Tertiary sequence of predominantly carbonates, overlaid by a Tertiary sequence of clays and turbiditic sandstones deposited in a foredeep environment (flysch) (IGRS-IFP, 1966). The Pindos zone was overthrust in the course of the Eocene by a complicated Jurassic to Early Eocene nappe stack of carbonates, an ophiolitic sequence and metamorphic rocks (e.g. Jacobshagen, 1986), which for the sake of convenience is indicated as the ''Upper Unit'' in the map of Fig. 4A.

The nappe pile is cross-cut at high angles by a series of Late Tertiary extensional and strike-slip faults (Fig. 4A). Some of these have been described before and two zones will be identified here. The Late Mio-Pliocene and still-active Aliakmon fault zone in Thessaly (Fig. 4A) has been recognised as a major NE–SW trending NW-verging normal fault zone. The Servia fault, which belongs to the Aliakmon fault zone, bounds the Kozani Basin (Fig. 4A). It has an estimated vertical displacement of 2100 m (Doutsos and Koukouvelas, 1998). The E–W trending Souli fault in Epirus (Fig. 4A) is a normal fault with a component of left-lateral strike-slip and has been active since some time after the Early Miocene until at least the Late Pleistocene (Boccaletti et al., 1997). A still-active NE–SW trending NW-verging normal fault is identified near Konitsa, forming the northern limit of the Timfi block (IGRS-IFP, 1966) (Fig. 4A), and a WNW-ENE trending, NNE-verging normal fault system, associated with the formation of the Gulf of Amvrakikos (Fig. 4A), is identified by Clews (1989). In the south-eastern part of NW Greece, the intramontane basins of Karditsa and Larissa (Fig. 4A)

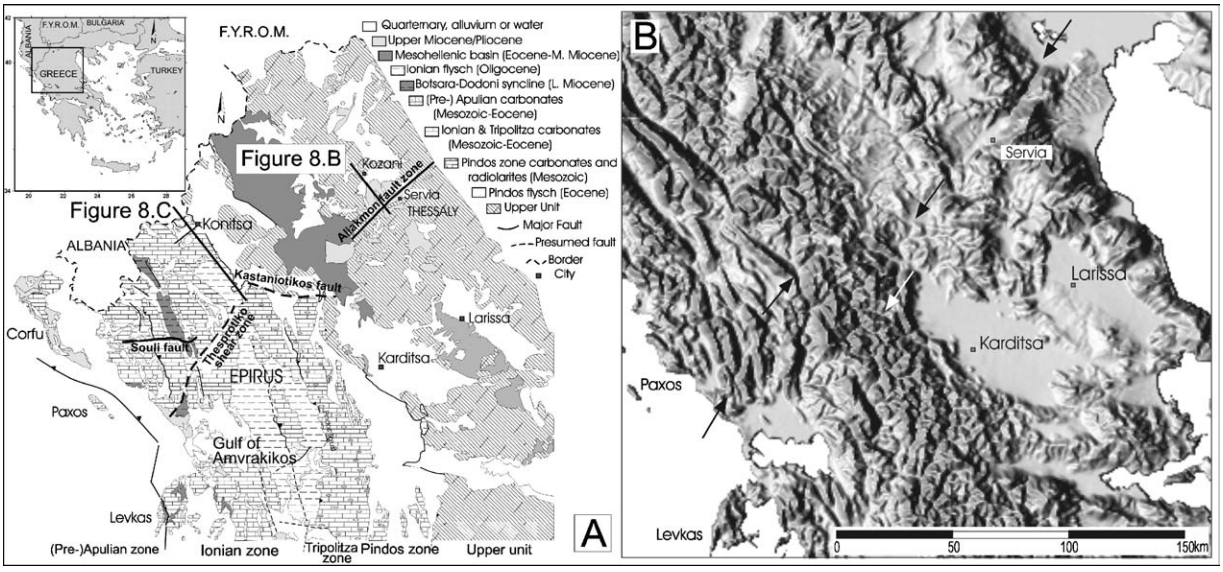

Fig. 4. North-western Greece study area. (A) Geologic map of north-western Greece with an inset indicating its position in Greece. Thick solid lines are locations of cross-sections in Fig. 8B and C. (B) Shaded relief model of original DEM (13× vertical exaggeration). Arrows indicate main lineaments in the NE–SW direction.

are filled with Late Neogene to Holocene terrestrial deposits.

Based on the geologic map of IGRS-IFP (1966) and Bornovas and Rontogianni-Tsiabaou (in press) and on field observations, two fault zones are identified that have not been mentioned before in the literature: the Thesprotiko fault zone runs NE–SW across Epirus and displaces a syncline filled with Lower Miocene sediments in a right-lateral sense by 15–20 km (Fig. 4A). Its age is post-Early Miocene. It interferes with the Kastaniotikos fault zone (Skourlis and Doutsos, in press), which is a WNW-ESE trending, north-verging normal fault zone, bringing the Upper Unit next to the Mesozoic carbonate sequence of the Pindos Zone (Fig. 4A) during an ill-defined time period after the Eocene.

In summary, the accentuated relief of NW Greece is associated with a complex, but well-known geologic structure. It is therefore a very suitable area to test the applicability of DTA methods to identify tectonic features from geomorphology on regional scale.

A DEM of NW Greece was obtained from the Global Land One-kilometer Base Elevation (GLOBE) model that has a 30 arc-s grid spacing and 1 m vertical resolution. The DTA of the DEM of NW Greece was carried out in combination with regional-size remote sensing (Landsat TM satellite images).

4. Results and discussion

4.1. Kali Basin, Hungary

4.1.1. Digital terrain analysis

The histogram of grid elevations shows systematic error in the DEM as spikes corresponding to the original contour lines at 10 m intervals (Jordan, 2003). A grey-scale elevation image shows a generally increasing elevation from SW to NE, indicating that the entire area is uniformly tilted towards the SW. Cross-sections across the basin in NE–SW direction also show the general dip of the area to the SW (Jordan et al., 2003).

Lineaments intersecting the entire basin in NE–SW direction are seen in the shaded relief image (b in Fig. 3B). The western boundary of the basin is marked by a series of volcanic cones aligning in a narrow N–S zone. N–S slope edges in the same direction are sharp (d in Fig. 3B). A third set of lineaments comprises NW–SE striking slope-breaks, and ridges and valleys cross-cutting the study area (c in Fig. 3B). Six-time vertical DEM exaggeration reveals a number of closed depressions in the basin area (h in Fig. 3B). Note that closed depressions are artefacts resulting from the spline interpolation error inherent to the initial preparation of the DEM as mentioned above.

Due to large systematic errors in the aspect derived from the original spline DEM, aspect calculations discussed below used a new DEM interpolated by TIN from the original contour lines. Systematic error shown as peaks in the aspect histogram at values of 45° azimuth is due to numerical derivation over a rectangular grid. The aspect rose diagram, calculated only for hilly areas with slopes of more than 1° (Fig. 5), displays two major directions: one facing SE (120°) and another pointing to the opposite direction (300°). The pronounced lack of land facets facing N and S suggests that E–W oriented morphological features are not characteristic for the area (compare to Fig. 3). Based on the rose diagram (Fig. 5), aspects were divided into two classes between 110° and 160°, and between 290° and 340°, respectively. The two aspect frequency peaks correspond to the flanks of the northern and southern hill ranges running in the NE–SW direction (Fig. 5). Related areas are elongated and bounded by sharp linear edges. Slopes of uniform aspect commonly have N–S and NW–SE edges, suggesting possibly tectonic control on morphology.

Uniform slope is expected where contour lines are equidistant in the original map. On the basis of cumulative percentage area-slope curves (Jordan, 2003), areas were classified as plain, hilly and mountaineous where slopes are $\leq 1°$, $1°$–$3°$ and $>3°$, respectively. A slope map displaying these classes shows sharp edges of the Kali Basin in the NE–SW, NW–SE and N–S directions.

The DEM, smoothed twice with a 3×3 moving average filter, was used as input for second-order derivatives. The resulting tangential curvature map displays valleys and ridges as white and black lines corresponding to positive and negative values, respectively (Jordan et al., 2003). The major NE–SW, NW–SE and N–S directions are apparent. Second-order derivatives in the X direction revealed prominent N–S linear features. The mixed second derivatives showed NE–SW and NW–SE running

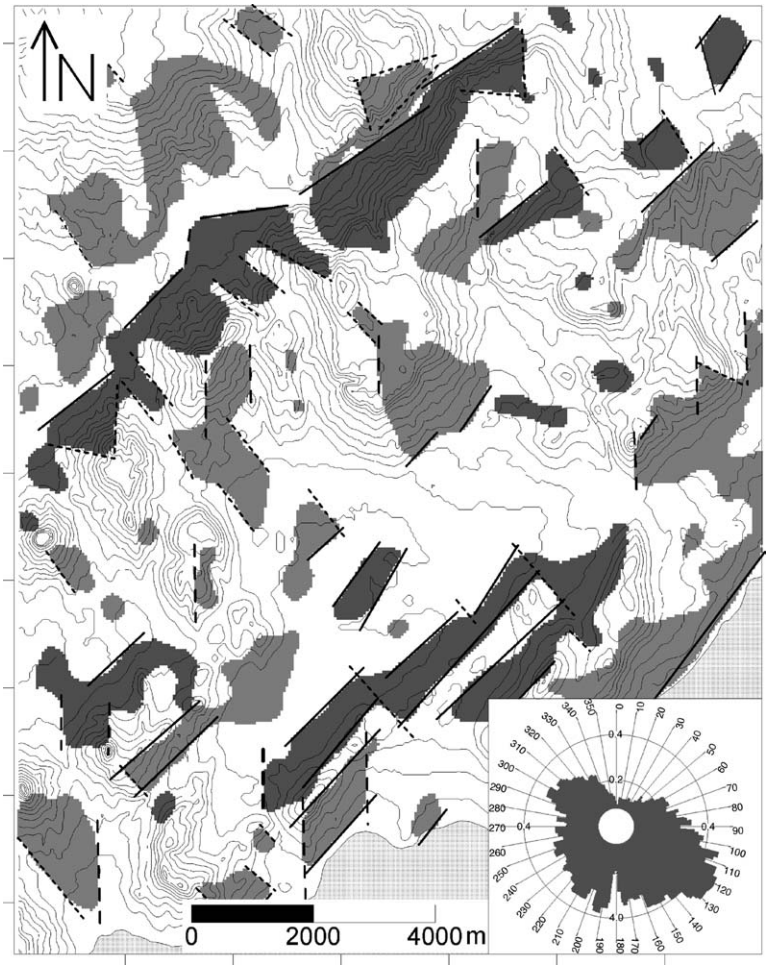

Fig. 5. Classified aspect image after 11 × 11 majority filtering. Dark and light shaded areas have aspects between 290° and 340°, 110° and 160°, respectively. Lines are drawn to highlight edges of hill slopes. Solid line: NE–SW direction; dashed line: N–S direction; dotted line: NW–SE direction. Elevation contours are also shown. Inset: rose diagram for aspect frequencies for slope > 1°.

linear features representing valleys, ridges and slope-breaks (Jordan et al., 2003).

The regional tilt of the area was analysed by linear trend surface fitting to the whole basin area, to sub-areas and to surface-specific points. An overall dip of about 1° to the SE is apparent if the trend plane is fitted to the Kali Basin area (below 140 m a.s.l. and defined by slope ≤1°) only. The orientation obtained is consistent with the SW tilt found in elevation analysis. Note that the same tilt is found in field measurements on Tertiary seashore sediments (Csillag, 2004).

Autocorrelation analysis was performed after extraction of a linear trend and subsequent 5 × 5 average smoothing of the DEM in order to study lineation (anisotropy) and periodicity due to faulting or folding (Jordan, 2003). The main anisotropy direction resulting from this analysis is parallel to the main NE–SW lineation orientation found by the DTA procedures outlined above. A variogram in the E–W direction for the drainage-based artificial DEM displays a periodic shape, suggesting that the N–S running valleys are periodic with about 3000 m separation on average. Inspection of a periodogram calculated for the same DEM reveals that the large-scale valleys dominate the morphology with a marked NE–SW orientation (Jordan, 2003).

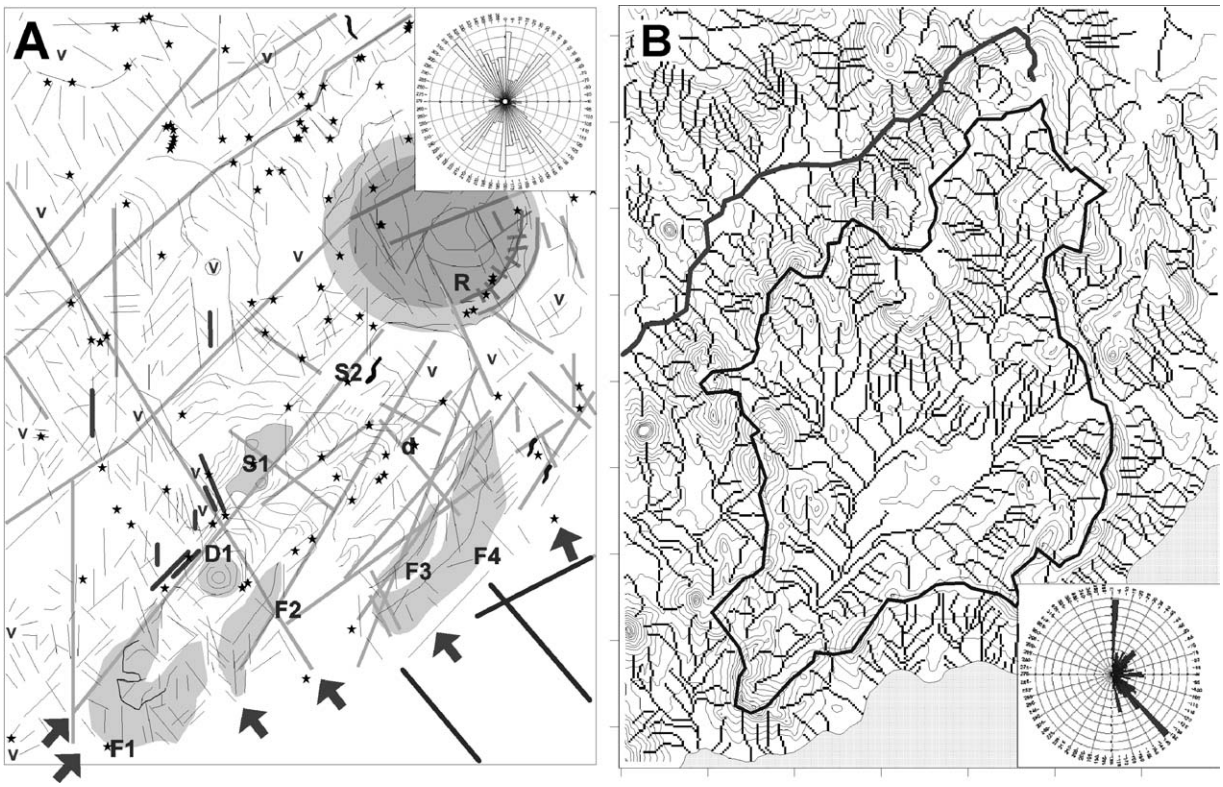

Fig. 6. (A) Lineament map. Black lines are line features (valleys, ridges and slope-breaks) digitised from terrain models. Grey polygons emphasise major morphological features. Thick light-grey lines show fracture lines shown in geological maps. Thick dark-grey lines show fracture lines recognised by other studies. Asterisks are springs. Large arrows show zones of springs. Key: D1, main depression; S1 and S2, S-shaped depressions; F1–F4, fold features; R, ring structure; d, asymmetric depressions; v, volcanic features. (For detailed analysis of these features see Jordan et al., 2003.) Inset: rose diagram of lineaments. (B) Watershed boundary of the Kali Basin (dark polygon) and valley lines for the study area defined by digital drainage extraction and watershed identification method. Valley line for the Eger Valley is highlighted (heavy grey line). Elevation contour lines are also overlaid. Inset: rose diagram for vectorised and smoothed channel segments with length > 300 m.

Lineaments defined by sharp grey-scale edges in the above images were digitised on screen (Fig. 6A). According to the rose diagram of lineaments (Fig. 6A), all linear features are oriented in one of the three main directions, i.e. (1) NE–SW, (2) N–S and (3) NW–SE. Valleys, ridgelines and slope-breaks corresponding to these three directions cross-cut the entire study area indicating a regional-size origin of these features. The three major orientations are consistent with the findings above. Since most of the valleys with these orientations cross-cut different rock types in the area, they cannot be related to bedding only. Digitally extracted drainage network and segment orientations are shown in Fig. 6B. The three major orientations are consistent with the findings above. The E–W petal in the rose diagram is interpreted here as an error caused by drainage extraction from a rectangular grid because grid-based drainage extraction is biased towards the four principle directions (Wilson and Gallant, 2000). The NW–SE petal is the longest although individual valley lines are shorter than in the other two directions. The low scatter of segments around these directions implies that related valley lines are well-defined.

4.1.2. Comparison with other data

Lineaments were extracted from a 1:100,000 DEM (100 m $\times$ 100 m resolution) covering half of the Balaton Highland in order to check if morphological features found in the Kali Basin are also present at a

regional size. The major lines in the three principle directions are all present in the smaller-scale DEM. NE–SW and NW–SE running linear valleys are predominant at the regional size and can be followed far beyond the study area (Jordan et al., 2003).

The gravity anomaly map of the area displays a pronounced NE–SW anisotropy (Vertesy and Kiss, 1995). Lineaments extracted from the gravity map using digital edge detection methods (Vertesy and Kiss, 1995) coincide with lineaments identified by the terrain modelling in this study. Previous studies (Nemeth and Martin, 1999) in the Kali Basin have recognised N–S orientation of volcanic structures such as basalt dykes associated with faults (Fig. 6A) along lineaments identified in this study. Digitised lineament maps of two remotely sensed image analysis studies using aerial photographs (Csillag, 1989) and satellite images (Marsi and Sikhegyi, 1985) also show a good correspondence with the DEM-based lineament map. In addition, springs align along some of the identified morphological lineaments corresponding to known fault lines (Fig. 6A). Detailed evaluation of geological data is provided elsewhere (Jordan et al., 2003).

4.2. NW Greece

4.2.1. Digital terrain analysis

For the digital tectonic geomorphology analysis of NW Greece, shaded relief models and differential geometry models, such as aspect, slope and curvatures models were used. Morphological cross-sections were calculated perpendicular to significant fault lines. Satellite images were draped over the DEM to create three-dimensional views. Lineaments observed in shaded relief, aspect, slope and curvature models were manually digitised on the screen. Notwithstanding the relatively poor resolution of the DEM used, the results provide an acceptable regional morphotectonic view of the study area.

The histogram of the grid elevation shows a systematic error in the DEM as small spikes corresponding to 50 m intervals resulting from the primary grid cell processing of the GLOBE model. Spikes at 10 and 110 m are related to the topographically low coastal regions in Epirus and Macedonia and to the Larissa and Karditsa basins in Thessaly, respectively (Fig. 4B).

The relief map shows high relief variability values in coastal regions and highly deformed areas in Epirus and along the borders of the Larissa and Karditsa basins.

Shaded relief models, calculated from DEMs smoothed by 3×3, 5×5, 7×7, 11×11 and 21×21 average filters, were displayed at four different illumination angles at 45° interval (Fig. 4B). The rose diagram of lineaments identified in these shaded relief maps shows a subtle trend to the north and east, while there are few lineaments with NE–SW to WSW–ENE orientations.

A lineament map of the aspect analysis was constructed on the basis of the presence of fault facets, ridge cut-offs and uniform dips of hill slopes (Fig. 7). Aspect maps were calculated from a DEM smoothed with a 7×7 average filter. Aspect angles were classed in 45° intervals and the classified aspect maps were subsequently filtered with a 5×5 pixel majority matrix to reduce noise and increase interpretability. For example, Fig. 7C illustrates an overlay map of two classified aspect images for the angles between 280° and 350°, one of which was filtered with a 3×3 majority matrix and the other with a 5×5 majority matrix. Fig. 7C illustrates the differences obtained when using different majority filters and shows that the choice of majority filter to obtain an optimal result is a matter of trial and error. On the other hand, the map in Fig. 7C shows that corresponding areas are elongate and bounded by sharply defined linear edges in the NE–SW direction. In general, the resulting lineament map of the aspect analyses illustrates two pronounced lineament orientations trending NW–SE and NE–SW (Fig. 7B).

Linear patterns in slope and curvature maps, which could be interpreted as slope-breaks, were used as criteria to construct a lineament map. This construction involved two steps. Firstly, the slope map, calculated from a DEM smoothed with a 5×5 moving average filter, was classified at $<4^\circ$, 4°–8°, 9°–11° and $>12^\circ$ angles, these values being based on slope-breaks in the cumulative slope histogram. Next, the calculation of tangential curvature maps and profile curvature maps was performed on a DEM smoothed twice with a 5×5 moving average filter. The trend of the lineaments on the slope and curvature maps is, in general, NNW–SSE to NW–SE only with few numbers of lineaments in other directions. Most of the

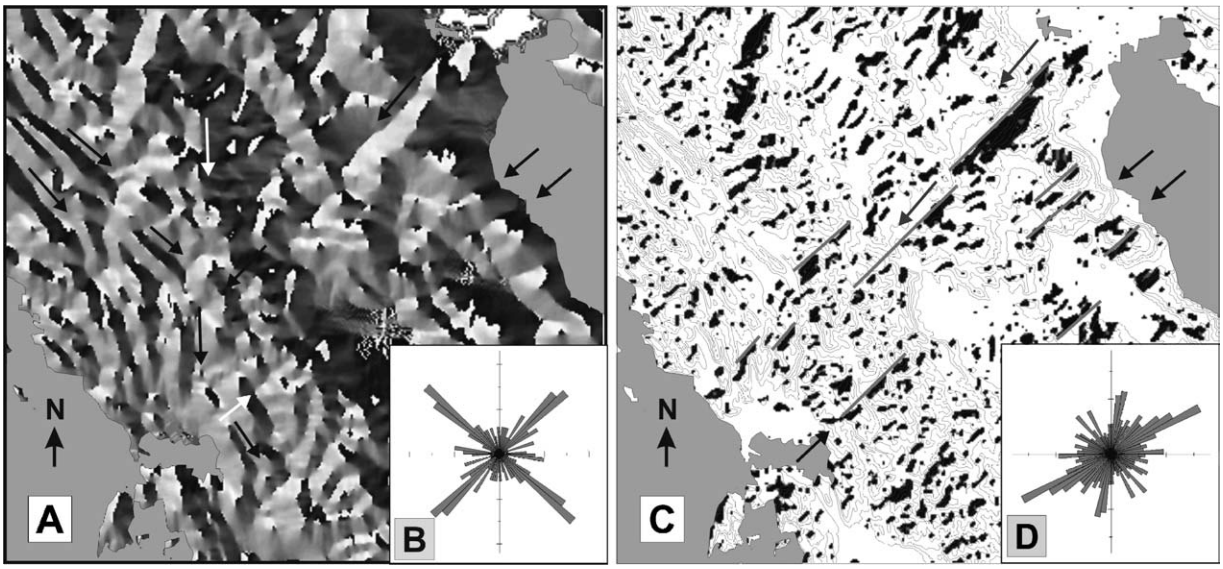

Fig. 7. (A) Grey-scale aspect image calculated from DEM smoothed with 7 × 7 moving average kernel. Arrows indicate main lineaments. (B) Rose diagram of lineaments identified in the aspect model (n = 125). (C) Classified aspect image for angles between 280° and 350° after majority filtering. Dark and light tones show 3 × 3 and 5 × 5 majority filtering, respectively. Arrows and lines indicate main lineaments in the NE–SW direction. (D) Rose diagram of lineaments identified in the satellite images (n = 848).

lineaments are located in Epirus and in the Olympos-Ossa mountain range to the east of Thessaly. The mixed second-order derivative map (Fig. 8A) illustrates a series of significant slope-breaks, which align along a series of NW–SE trending lineaments in Epirus.

The frequency (Fig. 7D) and length rose diagrams of the lineaments interpreted from satellite images illustrate a prominent NE–SW lineament orientation. Other but less prominent lineament orientations comprise NNE–SSW and NW to NNW lineament trends. There is also a fourth, less abundant set of lineaments in the E–W direction.

4.2.2. *Comparison of the lineaments with the geology*

To test whether the results of the DTA provide information on the geologic structure of the investigated area, the lineaments were compared with the geology. Especially in Epirus, the high number of NW–SE striking folds and thrusts are easily recognised on the lineament map of aspect analysis (Fig. 7A and B), as well as on slope and curvature maps. The cross-cutting fault systems of the Souli, Thesprotiko, Konitsa and Aliakmon faults and fault zones are recognised from the shaded relief and lineament maps of aspect models (Figs. 4B, 7B and C).

The morphological cross-sections (Fig. 8B and C) and perspective views of the Kozani Basin and the Pindos Mountains illustrate the geology associated with the sudden topographical changes identified by the DTA: the Konitsa fault and the interference zone of the Thesprotiko and Kastaniotikos fault zones coincide with the slope-breaks in the morphological cross-sections of Fig. 8C, and the jump in the (tectono-) stratigraphic level along the faults gives the relative vertical motion direction.

The WNW–ESE striking Kastaniotikos fault zone, which is easily recognised on the geologic map of Fig. 4A, is not well recognised by the DTA. This probably results from the fact that the NW–SE striking folds of the southern Pindos Mountains are not cut-off to form fault facets, but form more gentle drag folds along the WNW–ESE striking Kastaniotikos fault zone. Moreover, the elevation on both sides of the fault zone is rather comparable, although the lithology is different. Thus, no large topographic changes can be identified.

Comparison of the results of the DTA with the known geology from NW Greece indicates that the

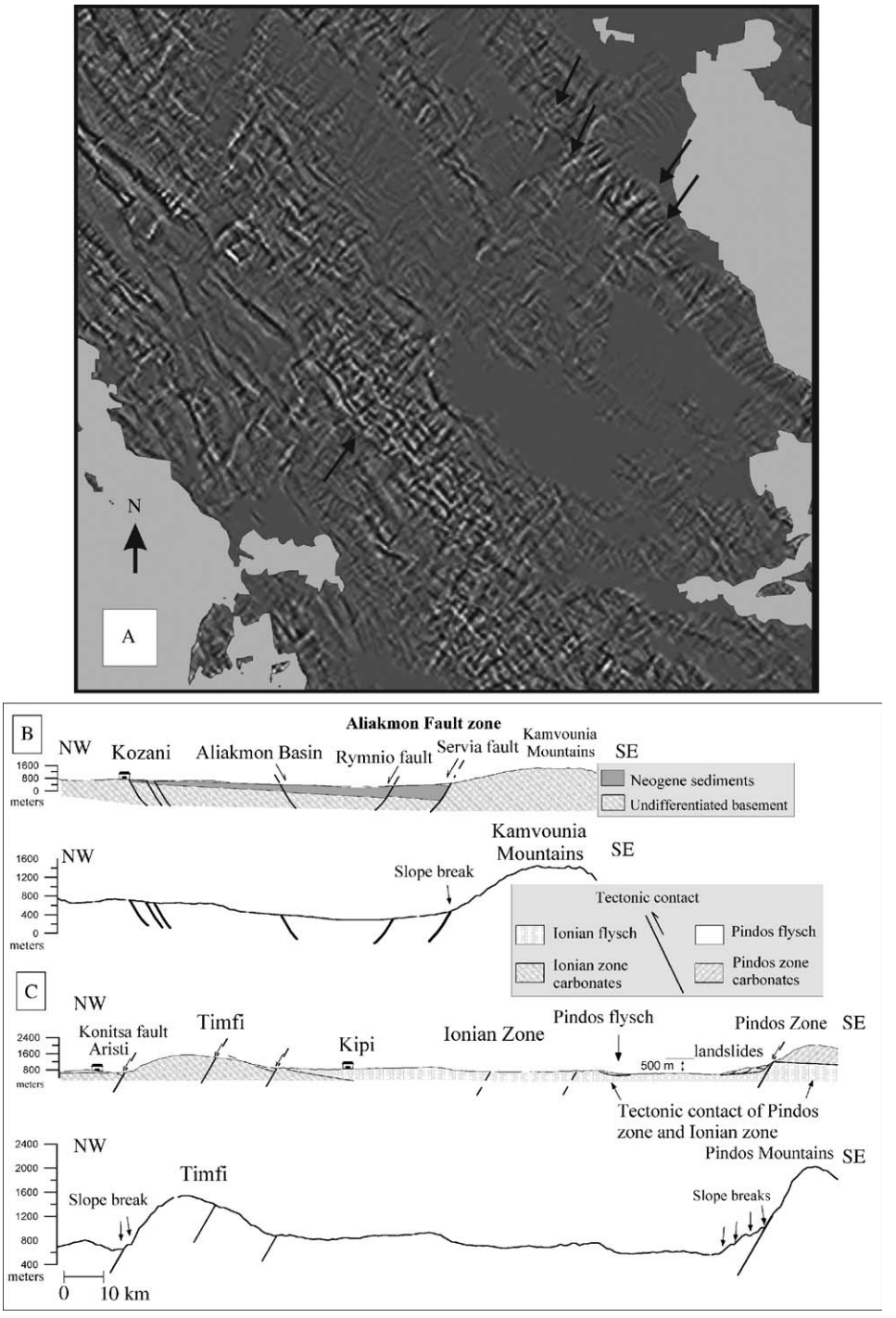

Fig. 8. (A) Grey-scale image of mixed second-order derivatives. Arrows indicate main lineaments in the NE–SW direction. (B and C) Geological and morphological cross-sections through the Kozani region (based on Doutsos and Koukouvelas, 1998) and Pindos Mountains, respectively. For location of sections see Fig. 4A.

major faults and fault systems correspond (in most cases) to clear lineaments. Much more lineaments were recognised, however, than faults have been identified in the field. It is tentatively concluded that these lineaments do correspond to yet unknown faults or folds. The limited field check available was very successful, and it is likely that other lineaments that were not visited can be readily identified in the field.

5. Conclusions

The systematic digital terrain analysis procedure was designed to use various tools in combination to extract morphotectonic features and parameters from DEMs (Jordan and Csillag, 2003). The individual procedures were in fact used at various stages and outputs were subsequently updated. Image processing techniques, such as smoothing (low-pass filtering), image filtering or histogram slicing (terrain attribute classification) were carried out at almost all stages of the analysis.

Both on local and regional scales, aspect analysis proved to be a powerful technique to identify tectonic lineaments and to characterise the structural properties of faults on a morphological basis. Slope-breaks are the second derivatives in the gradient direction, so high values of profile curvature could be used to identify sudden changes in the slope angle in the study areas.

The two-dimensional autocorrelogram provided a measure of anisotropy due to tectonics in the Kali Basin. Spectral analysis performed on the digitally extracted drainage network also provided a measure of terrain anisotropy at different scales consistent with the other results. A tectonic origin of valleys was demonstrated by a periodic variogram calculated from an extracted channel network in the local-scale study for the Kali Basin (Jordan, 2003). From these data, it could be inferred that the geomophology of the Kali Basin was affected by tectonic processes, with most of the faults recognisable as regional morphological features in the regional-scale shaded relief model.

Orientations calculated from the lineament maps derived for NW Greece showed the same directional trends as lineaments in the satellite images. Comparison with the geology indicated that the major fold and fault zones were easily recognised by the DTA methods applied. Various pre-processing methods such as smoothing of DEM or majority filtering of classified terrain attribute maps greatly enhanced the analysis of the noisy regional-scale DEM of Greece. The DTA of NW Greece illustrated that major and minor structures could easily be identified in large areas of land and that it is, hence, a powerful tool to obtain a quick overview of the structure of an area.

The use of DTA methods proposed in this study (1) yielded reproducible results and (2) provided a quantitative description of morphotectonic landforms (Jordan and Csillag, 2003). Reproducibility is an improvement as compared with traditional morphological map analysis and visual image interpretation. Quantitative geometric characterisation of landforms based on DEM analysis is an advantage when compared with digital processing of remotely sensed images or analysis of grey-scale terrain images. Geometric terrain characterisation facilitates measurement of landforms and hence their comparison on a quantitative basis. The presented digital terrain analysis procedure thus provided a systematic and consistent framework for digital tectonic geomorphology.

Acknowledgements

Reinoud Vissers is gratefully thanked for critical reading of the manuscript. Thanks to Emőke Jocháné Edelényi and György Tóth of the Geological Institute of Hungary for providing facilities for the preparation of this paper.

References

Aubouin, J., 1957. Essai de corrélation stratigraphique de la Grèce occidentale. Bull. Soc. Géol. France 7, 281–304.

Baas, J.H., 2000. EZ-ROSE: a computer program for equal-area circular histograms and statistical analysis of two-dimensional vectorial data. Comput. Geosci. 26, 153–166.

Boccaletti, M., Caputo, R., Mountrakis, D., Pavlides, S., Zouros, N., 1997. Paleoseismicity of the Souli Fault, Western Greece. J. Geodyn. 24, 117–127.

Bonneau, M., 1984. Correlation of the Hellenic Nappes in the south–east Aegean and their tectonic reconstruction, in: Dixon, J.E., Robertson, A.H.F. (Eds.), The Geological Evolution of the Eastern Mediterranean. Geol. Soc. Lond., Spec. Pub. 17, 517–527.

Bornovas, I., Rontogianni-Tsiabaou, T. Geological Map of Greece, second ed., 1:500.000, Institute of Geology and Mining Exploration, Athens, in press.

Budai, T., Csaszar, G., Csillag, G., Dudko, A., Koloszar, L., Majoros, G., 1999. Geology of the Balaton Highland. Geological Institute of Hungary, Budapest (in Hungarian with English summary).

Burbank, D.W., Anderson, R.S., 2001. Tectonic Geomorphology. Blackwell Science, Malden.

Byrd, J.O.D., Smith, R.B., Geissman, J.W., 1994. The Teton fault, Wyoming: neotectonics, and mechanisms of deformation. J. Geophys. Res. 99 (B10), 20095–20122.

Chorowicz, J., Kim, J., Manoussis, S., Rudant, J., Foin, P., Veillet, I., 1989. A new techniqe for recognition of geological and geomorphological patterns in digital terrain models. Remote Sens. Environ. 29, 229–239.

Chorowicz, J., Breard, J., Guillande, R., Morasse, C., Prudon, D., Rudant, J., 1991. Dip and strike measured systematically on digitised three-dimensional geological map. Photogrammetric Eng. Remote Sens. 57, 431–436.

Chorowicz, J., Parrot, J., Taud, H., 1995. Automated patter-recognition of geomorphic features from DEMs and satellite images. Z. Geomorphol., Supplementary Band 101, 69–84.

Chorowicz, J., Collet, B., Bonavia, F.F., Mohr, P., Parrot, J.F., Korme, T., 1998. The Tana basin, Ethiopia: intra-plateau uplift, rifting and subsidence. Tectonophysics 295, 351–367.

Chorowicz, J., Dhont, D., Gundogdu, N., 1999. Neotectonics in the eastern North Anatolian fault region (Turkey) advocates crustal extension: mapping from SAR ERS imagery and Digital Elevation Model. J. Struct. Geol. 21, 511–532.

Clark, C.D., Wilson, C., 1994. Spatial analysis of lineaments. Comput. Geosci. 20, 1237–1258.

Clews, J.E., 1989. Structural controls on basin evolution: Neogene to Quarternary of the Ionian zone, Western Greece. J. Geol. Soc. Lond. 146 (3), 447–457.

Collet, B., Taud, H., Parrot, J.F., Bonavia, F., Chorowicz, J., 2000. A new kinematic approach for the Danakil block using a Digital Elevation Model representation. Tectonophysics 316, 343–357.

Csillag, G., 1989. Lineament map of the Balaton Highland. Research Report, Orszagos Foldtani es Geofizikai Adattar, Hungary.

Csillag, G., 2004. Geomorphological levels of the Kali Basin and vicinity. Foldtani Intezet Evi Jel. 2002. Evrol., Budapest, pp. 95–110 (in Hungarian).

Curran, P.J., 1988. The semivariogram in remote sensing: an introduction. Remote Sens. Environ. 24, 493–507.

Davis, J.C., 1986. Statistics and Data Analysis in Geology. John Wiley and Sons Co., New York.

Deffontaines, B., Chorowicz, J., 1991. Principles of drainage basin analysis from multi-source data: application to the structural analysis of the Zaire Basin. Tectonophysics 194, 237–263.

Doornkamp, J.C., 1972. Trend-surface analysis of planation surfaces, with an East-African case study. In: Chorley, R.J. (Ed.), Spatial Analysis in Geomorphology, Methuen, London, pp. 247–281.

Doutsos, T., Koukouvelas, I., 1998. Fractal analysis of normal faults in northwestern Aegean area, Greece. J. Geodyn. 26 (2–4), 197–216.

Drury, S.A., 1987. Image Interpretation in Geology. Allen and Unwin, London.

Evans, I.S., 1972. General geomorphometry, derivatives of altitude, and descriptive statistics. In: Chorley, R.J. (Ed.), Spatial Analysis in Geomorphology, Methuen, London, pp. 17–90.

Evans, I.S., 1980. An integrated system for terrain analysis for slope mapping. Z. Geomorphol. 36, 274–295.

Florinsky, I.V., 1996. Quantitative topographic method of fault morphology recognition. Geomorphology 16, 103–119.

Florinsky, I.V., 1998. Combined analysis of digital terrain models and remotely sensed data in landscape investigations. Prog. Phys. Geogr. 22, 33–60.

Florinsky, I.V., 2000. Relationship between topographically expressed zones of flow accumulation and sites of faults intersection: analysis by means of digital terrain modelling. Environ. Modell. Software 15, 87–100.

Fraser, A.J., Huggins, P., Cleverley, P., Rees, J.L., 1995. A satellite remote-sensing technique for geological horizon structure mapping. SEG Annual Meeting, Expanded Technical Program Abstracts with Biographies.In: Society of Exploration Geophysicists. Tulsa, OK, United States pp. 65, 134–137.

Frisch, W. (Ed.), 1997. Tectonic Geomorphology. In Proceeding of the Fourth Int'l. Conf. on Geomorphology, Z. Geomorphol. N. F., Supplementary Band, 118.

Garbrecht, J., Martz, L.W., 1995. Agricultural Research Service Publication NAWQL 95-3, in: TOPAZ: An Automated Digital Landscape Analysis Tool For Topographic Evaluation, Drainage Identification, Watershed Segmentation and Subcatchment Parametrisation: TOPAZ User Manual. U.S. Department of Agriculture, 95-3, Washington, DC.

Goldsworthy, M., Jackson, J., 2000. Active Normal Fault Evolution in Greece Revealed by Geomorphology and Drainage Patterns, 157. Geological Society, Special Publication, London, pp. 967–981.

Gonzalez, R.C., Woods, R.E., 1993. Digital Image Processing. Addison-Wesley Publishing Company, New York.

Guth, P.L., 1997. Tectonic geomorphology of the White Mountains, eastern California, in: Geological Society of America, 1997 Annual Meeting, Abstracts with Programs, vol. 29, p. 235. Geological Society of America (GSA). Boulder, CO, United States.

Harrison, J.M., Lo, C., 1996. PC-based two-dimensional discrete spectral transform programs for terrain analysis. Comput. Geosci. 22, 419–424.

Hobbs, W.H., 1912. Earth Features and their Meaning. Macmillian Co., New York.

IGRS-IFP, 1966. Étude géologique de l'Épire (Grèce nord-occidentale). Editions Technip., Paris, 306 p.

ILWIS, 1997. The Integrated Land and Water Information System. Reference Guide. ILWIS Department, ITC, Enschede.

Jacobshagen, V., 1986. Geologie von Griechenland. Beiträge zur regionalen Geologie der Erde, 19. Berlin-Stuttgart, Bornträger, p. 363.

Jordan, G., 2003. Morphometric analysis and tectonic interpretation of digital terrain data: a case study. Earth Surf. Process. Landforms 28, 807–822.

Jordan, G., Csillag, G., 2001. Digital terrain modelling for morphotectonic analysis: a GIS framework. In: Ohmori, H. (Ed.),

DEMS and Geomorphology. Special Publication of the Geographic Information Systems Association, vol. 1. Nihon University, Tokyo, pp. 60–61.

Jordan, G., Csillag, G., 2003. A GIS framework for morphotectonic analysis—a case study. Proceedings of Fourth European Congress on Regional Geoscientific Cartography and Information Systems, 17–20 June 2003. Bologna, Italy. Proceedings, vol. 2. Regione Emilia-Romana, Servizio Geologico, Bologna, pp. 516–519.

Jordan, G., Csillag, G., Szucs, A., Qvarfort, U., 2003. Application of digital terrain modelling and GIS methods for the morphotectonic investigation of the Kali Basin, Hungary. Z. Geomorphol. 47, 145–169.

Jordan, G., Schott, B., 2005. Application of wavelet analysis to the study of spatial pattern of morphotectonic lineaments in digital terrain models. A case study. Remote Sensing of Environment, in press.

Keller, E.A., Pinter, N., 1996. Active Tectonics: Earthquakes, Uplift and Landforms. Prentice Hall, New Jersey.

Koike, K., Nagano, S., Kawaba, K., 1998. Construction and analysis of interpreted fracture planes through combination of satellite-image derived lineaments and digital elevation model data. Comput. Geosci. 24, 573–583.

Le Turdu, C., Coussement, C., Tiercelin, J.-J., Renaut, R.W., Rolet, J., Richert, J.-P., Xavier, J.-P., Coquelet, D., 1995. Rift basin strucure and depositional patterns interpreted using 3D remote sensing approach: the Barongo and Bogoria Basins, Central Kenya Rift, East Africa. Bull. Centres Récherches 19, 1–37.

Lillesand, T.M., Kiefer, R.W., 1994. Remote Sensing and Image Interpretation. Wiley Co., New York.

Marsi, I., Sikhegyi, F., 1985. Application of satellite images and aerial photographs for bauxite exploration. Foldtani Kutatas 28, 65–70 (in Hungarian).

Martz, L.W., Garbrecht, J., 1992. Numerical definition of drainage networks and subcarchment areas from digital elevation models. Comput. Geosci. 18, 747–761.

McCullagh, M.J., 1988. Terrain and surface modelling systems: theory and practice. Photogrammetric Rec. 12, 747–779.

Mitášová, H., Hofierka, J., 1993. Interpolation by regularised spline with tension: II. Application to terrain modelling and surface geometry analysis. Math. Geol. 25, 655–657.

Moore, I.D., Lewis, A., Gallant, J.C., 1993. Terrain attributes: estimation methods and scale effects. In: Jakeman, A.J., Beek, M.J., McAleer, M.J. (Eds.), Modelling Change in Environmental Systems. John Willey and Sons, London.

Nemeth, K., Martin, U., 1999. Small-volume volcanoclastic flow deposits related to phreatomagmatic explosive eruptive centers near Szentbekalla, Bakony-Balaton Highland Volcanic Field, Hungary: pyroclastic flow or hydroclastic flaw? Foldtani Kozlony 129, 393–417.

Onorati, G., Poscolieri, M., Ventura, R., Chiarini, V., Crucillá, U., 1992. The digital elevation model of Italy for geomorphology and structural geology. Catena 19, 147–178.

Peucker, T.K., Douglas, D.H., 1975. Detection of surface-specific points by local parallel processing of discrete terrain elevation data. Comput. Graphics Image Process. 4, 375–387.

Prewitt, J.M.S., 1970. Object enhancement and extraction. In: Lipkin, B.S., Rosenfeld, A. (Eds.), Picture Processing and Psychopicotoics. Academic Press, New York, pp. 75–149.

Prost, G.L., 1994. Remote sensing for geologists. In: A Guide to Image Interpretation, Gordon and Breach Science Publishers, Amsterdam.

Ramsay, J.G., Huber, M.I., 1987. The Techniques of Modern Structural Geology. Vol. 2. Folds and Fractures. Academic Press, London.

Riley, C., Moore, M.C.M., 1993. Digital elevation modelling in a study of the neotectonic geomorphology of the Sierra Nevada, southern Spain. Z. Geomorphol. N.F., Suppl. Band 94, 25–39.

Salvi, S., 1995. Analysis and interpretation of Landsat synthetic stereo pair for the detection of active fault zones in the Abruzzi Region (Central Italy). Remote Sens. Environ. 53, 153–163.

Sauter, D., De-Frainpont, P., Ruhland, M., 1989. Image processing applied to digital elevation models: a useful tool for structural studies, in: Proceedings of the Thematic Conference on Geologic Remote Sensing, vol. 7. Ann Arbor: Environmental Research Institute of Michigan, Michigan, pp. 1073–1080.

Sharpnack, D.A., Akin, G., 1969. An algorithm for computing slope and aspect from elevations. Photogrammetric Eng. 35 (3), 247–248.

Siegal, B.S., Gillespie, A.R., 1980. Remote Sensing in Geology. John Wiley and Sons, New York.

Simpson, D.W., Anders, M.H., 1992. Tectonics and topography of the Western United States—an application of digital mapping. GSA Today 2, 118–121.

Skourlis, K., Doutsos, T. The Pindos fold-and-thrust belt (Greece): Inversion kinematics of a possible continental margin. Int. J. Earth. Sci., in press.

Trunko, L., 1995. Geology of Hungary. Gebrüder Borntraegen, Berlin.

Vertesy, L., Kiss, J., 1995. Report on the environmental investigations in 1993. Research Report, Eötvös Lorand Geophysical Institute, Budapest.

Wells, N.A., 1999. ASTRA.BAS: a program in QuickBasic 4.5 for exploiting rose diagrams, circular histograms and some alternatives. Comput. Geosci. 25, 641–654.

Way, D.S., 1973. Terrain Analysis. A Guide to Site Selection Using Aerial Photographic Interpretation. Dowden, Hutchinson & Ross Inc., Pennsylvania.

Wilson, J.P., Gallant, J.C., 2000. Terrain Analysis. Principles and Applications. John Wiley & Sons, London.